Science Advances
AAAS

Supplementary Materials for

Loss of metabolic fitness drives tumor resistance after CAR-NK cell therapy and can be overcome by cytokine engineering

Li Li *et al.*

Corresponding author: Katayoun Rezvani, krezvani@mdanderson.org; Ken Chen, kchen3@mdanderson.org

Sci. Adv. **9**, eadd6997 (2023)
DOI: 10.1126/sciadv.add6997

This PDF file includes:

Supplementary Methods

Study design

The study's objective was to investigate the kinetics of function and the in vivo evolution of adoptively-infused CAR-NK cells in the context of lymphoma treatment and to study the mechanisms associated with resistance to CAR-NK cell therapy and disease relapse. To accomplish this, we designed in vivo studies in a non-curative Raji lymphoma model by systematically tracking the evolution of both the tumor and CAR-NK cells collected from the liver, spleen, blood, and bone marrow from animals in each of our treatment groups (NT-NK, CAR19 NK, CAR19/IL-15 alone, 2-infusion of CAR19/IL-15 and 1-infusion of CAR19/IL-15 NK cells) by using single cell transcriptomic and proteomic approaches. Lastly, we investigated whether these same observations were true in the clinical setting by conducting an unbiased single-cell gene expression analysis of CAR-NK cells and B cells from two patients with CD19+ lymphoma treated with adoptive CAR-NK cell therapy (NCT03056339). All subjects gave fully informed and written consent. All studies were performed in accordance with the Declaration of Helsinki.

Cell lines, primary cells and culture conditions

The CD19+ Raji Burkitt lymphoma cell line (CCL-86), and the K562 erythroleukemia cell line (CRL-3344) were obtained from the American Type Culture Collection (Manassas, VA). K562 cells were retrovirally transduced to co-express 4-1BBL, CD48, and membrane-bound interleukin (IL)-21 and served as universal antigen presenting cells (uAPC) for *in vitro* NK cell expansion (*30*). Raji and K562 cells were cultured in RPMI-1640 (Invitrogen) supplemented with 10% fetal bovine serum (FBS; HyClone), 1% penicillin-streptomycin, and 1% GlutaMAX™. Peripheral blood samples used in this study were collected from two patients treated on a clinical trial of adoptive therapy with cord blood (CB)-derived NK cells expressing iC9/CAR19/IL-15 (CAR19/IL-15) at MD Anderson Cancer Center as previously reported (NCT03056339). All patients gave informed consent following Institutional Review Board (IRB)-approved protocols. All studies were performed in accordance with the Declaration of Helsinki.

CAR-engineered NK cell production

$CD56^{+}CD3^{-}$ NK cells isolated from cord blood units obtained from the MD Anderson Cancer Center Cord Blood Bank were purified using an NK negative isolation kit (Miltenyi Biotec), and co-cultured with irradiated (100 Gy) uAPCs at a 1:2 (NK cells: uAPC) ratio in complete stem cell growth medium (SCGM), supplemented with 200 U/ml recombinant human IL-2 (Proleukin). On Day 4 post uAPC stimulation, fresh NK cells were purified again and transduced with retroviral vectors expressing the CAR constructs described above.

NK cell cytotoxicity assay

Chromium release assay

To measure NK cell cytotoxicity, NT, IL-15, CAR19 and CAR19/IL-15 NK cells were co-cultured with ^{51}Cr-labeled Raji or ^{51}Cr-labeled K562 targets at different effector: target (E:T) ratios (*15*).

Seahorse assay

The extracellular acidification rate (ECAR) was measured using the Agilent Seahorse XFe96 Analyzer (Agilent) following the manufacturer's protocol as previously described (*29*). In **Fig. 1G**, NT, CAR19 and CAR19/IL-15 NK cells were assayed either alone or purified after 2 hours of co-culture with Raji targets followed by the Seahorse assay. **Fig. S6A** is an independent experiment where ECAR was measured by Seahorse assays using 2 g/L D-glucose, 2.5 μM oligomycin and 100 mM 2-Dexyglucose (2-DG) followed by live cell counting using Hoechst 33342 (Invitrogen) dye in Cytation 1 cell imaging multi-mode reader (Agilent).

Xenograft lymphoma model

Expanded NT or CAR-transduced NK cells (10×10^{6}/mouse) were injected through the tail vein on day 0. We started with 13-15 mice per group for the single infusion in vivo experiment (Fig. 2) and 15 mice per group for the double infusion in vivo experiment (Fig. 6). Five (5) mice per group were followed for survival

and tumor cells were quantified weekly using Living Image software as previously described (*15*). Additionally, 8-10 mice were followed for single cell analysis with 2 mice per group sacrificed at 4 timepoints (days 7, 14, 21 and 28 for the NT and CAR19 groups) for the experiments presented in Fig. 2 or 5 timepoints (days 7, 14, 21, 28, and 35 and days 14, 21, 28, 35 and 61 for double infusion group for the CAR19/IL-15 group) for the experiments presented in Figs. 2 and 6 . At each time point, we collected liver, spleen, blood and bone marrow, and cells were harvested and cryopreserved for later analysis by scRNA-seq and mass cytometry. The experimental schema is shown in **Figs. 2A and 3H** for single infusion experiments, and **Fig. 6A** for double infusion. Mice were euthanized according to the Protection of Animals Act.

For the two infusions mouse model (**Fig. 6A**), mice received FFluc-labeled Raji tumor cells alone, or Raji plus 2 infusions of 10 x 10^6 NT-NK or 2 infusions of 10 x 10^6 CAR19/IL-15 NK cells two weeks apart. Mice received the first infusion (from donor 1) on day 0, and the second infusion (from donor 2) on day 14. For mass cytometry studies, human NK cells were gated on hCD45+, then donor 1 and donor 2 NK cells were identified by the HLA type: donor 1 (HLA-A3+) and donor 2 (HLA-A2+). The gating strategy is shown in **Fig. S8**.

Single cell RNA sequencing (scRNA-seq)

Sample preparation for scRNA-seq

Cryopreserved tumor and NK cells isolated from mouse tissues were thawed and stained with antibodies against human CD45 (Clone HI30: Biolegend), CD3 (Clone HIT3a: Biolegend), CD56 (Clone HCD56: Biolegend) and CD20 (Clone 2H7: Biolegend). NK cells were identified as human CD45+CD3-CD56+ and tumor cells as human CD45+CD20+CD3-.

scRNA-seq analysis

Single-cell libraries were prepared using the 10X Genomics Chromium 3' scRNA-seq according to manufacturer's protocol. Briefly, single cells were partitioned into Gel beads in Emulsion (GEM) in the

10X Chromium Controller instrument followed by cell lysis, barcoded reverse transcription of RNA, and amplification. Subsequent to 5' adapter ligation, samples were indexed for sequencing. On average, 5000 cells were loaded on each channel, resulting in recovery of an average of 1200 cells/sample. Libraries were sequenced on Illumina (NovaSeq6000, SP flow cell -100 cycle kit per pool), Paired end reads: read 1, 28 bp, Read 2, 91 bp.

scRNA-seq data pre-processing

Data pre-processing was performed in Cell Ranger, the default analysis pipeline recommended by 10x Genomics, to de-multiplex raw base call files to FASTQ files, and subsequently align reads to human genome (GRCh 38) with the default parameters. All 18 samples were merged into a single data matrix, which was then loaded into Seurat v3.0 for analysis. Cells with fewer than 200 detected genes, or with greater than 10% mitochondrial genes were excluded. After log-normalization, confounding factors including number of detected genes and mitochondrial gene proportion were regressed against. Additional quality control of the measured cells was performed based on known cell type markers as shown in **Figs. S2-3**. Cells having *NKG7*>0 and *CD19*=0 were identified as NK cells, and cells having *NKG7*=0 and *CD19* or *MS4A1*>0 were identified as tumor cells. The NK cells located in tumor dominated clusters and tumor cells located in NK dominated clusters were removed.

Doublet detection

DoubletFinder v3 (*31*) was used to identify doublet cells. Doublet proportion for each cell was estimated with pN (the number of generated artificial doublets) set as 0.25 and pK (neighborhood size used to compute the number of artificial nearest neighbors) selected at the peak of the BC_{MVN} distribution.

RNA-sequence library preparation and sequencing from single cells from patient samples

PBMCs from the recipients of CAR19/IL-15 NK cell therapy (*11*) were enriched by Ficoll-hypaquse density gradient centrifugation, kept frozen in the vapor phase of liquid nitrogen, and thawed from the time

points as indicated. Thawed cells were rested for 20 min in a humidified incubator at 37 degree Celsius in the presence of 5% CO2, washed in PBS with 1% BSA, and stained for a viability dye (Tonbo BioScience), CD19 (Clone HIB19: BD Bioscience), CD33 (Clone P67.6: BD Bioscience), CD14 (Clone M5E2: BD Bioscience), CD3 (Clone SK7: BD Bioscience),CD20 (Clone 2H7: BD Bioscience), CD56 (Clone N901: BeckMan Coulter), CD45 (Clone J33: BeckMan Coulter). CAR was detected on donor HLA positive, CD3-, CD16+ and CD56+ cells by using the fluorophore-tagged F(ab)2 fragment against Human IgG (Jackson Immunoresearch) as described previously (*11*). Single cells from the donor NK cell population, or from B cells of the patients were sorted into each well of a 96 well plate with lysis buffer (10 μl of TCL buffer, Qiagen and 1% 2-mercaptoethanol: Sigma). The plates were spun down at 400xg for 5 minutes at 4 degree Celsius and immediately stored at -80°C until library preparation. cDNA was synthesized as described by the Smart-Seq2 protocol from Picelli *et al.* (*32*). Briefly, RNA was purified using RNAClean XP beads (Beckman Coulter) and reverse transcribed to cDNA using Maxima RNAse H-minus (ThermoFisher) in the presence of biotinylated oligo-dT30VN, biotinylated template-switching oligonucleotides, and betaine. Next, a PCR pre-amplification step was done with KAPA HiFi HotStart Ready Mix (Roche Diagnostics) and biotinylated ISPCR primers. DNA products were further purified with Agencourt XP DNA beads, and the concentration of each sample was quantified by Qubit dsDNA HS Assay kits (Invitrogen). Quality of samples was analyzed on a 2100 Bioanalyzer using a High Sensitivity DNA Kit (Agilent Technologies). 0.15 ng of each sample was tagmented and Nextera index adapters were used for barcoding according to the Illumina Nextera XT DNA sample preparation kit (Illumina).

For sequencing, single cell libraries were pooled equally, purified using AMPure XP beads and analyzed on a 2100 Bioanalyzer. Pooled libraries were denatured and diluted to 1.8pM prior to sequencing using 75 cycle paired-end kit on a NextSeq 500 (Illumina) with an average sequencing depth of 1 million reads per cell. The obtained mRNA sequencing data was demultiplexed into individual FASTQ files followed by alignment to the human reference genome hg19.

Single-cell RNA unsupervised clustering and dimension reduction

To explore the transcriptomics of the different engineered NK cells products, we performed clustering and dimension reduction on cells from pre-infusion only (**Fig. 1**). To explore the interaction between NK cells and tumor cells over time, we performed the same analysis by pooling all the cells together (**Fig. 3**). Specially, the top 2,000 highly variable genes were obtained, and principal component analysis (PCA) was performed. The top 20 Principal components (PCs) were used to perform clustering (with a resolution of 0.5) based on k-nearest neighbors (KNN) method in Seurat V3.0 (*33*). The non-linear dimensional reduction technology uniform manifold approximation and projection (UMAP) (based on 20 PCs) was used to project the cells onto a two-dimensional space.

Differential expression gene analysis

Additional quality control of the measured cells was performed based on known cell-type markers shown in **fig. S3**. Cluster specific upregulated genes were determined by "*FindAllMarkers*" function in Seurat (*only.pos*=*TRUE*, *logfc.threshold*=0.25; *p_val_adj*=10^{-5}). We generated heatmaps displaying the expression profiles of the top 20 genes for each cluster using "*ComplexHeatmap*" R package (*34*). To identify enriched pathway for each cluster, we identified cluster specific genes and over-expressed genes as defined above and performed pathway enrichment using the enricher tool (*35*) with the *HALLMARK* option and Fisher's exact test. Significant pathways were identified at FDR-adjusted P value < 0.01.

Proliferation score

Proliferation score was generated using the metaPCNA signature from Venet et al. (*36*) and scored using the AddModuleScore function in Seurat.

Monocle3 trajectory analysis

Trajectory analysis was performed using Monocle3 (*37*). Gene expression of all NK cell was pre-processed using the function *preprocess_cds*, Dimensionality reduction during pre-processing was performed using 15 PCA dimensions. The trajectory was learned using the function *learn_graph*. Pseudotime was computed

using the indicated node as the root (**Fig. 5A**). The node for the trajectory dominated by post-infusion cells (post-infusion trajectory) was selected at N5 as it represents early timepoints in CAR/IL-15 groups which is later replaced by N6 and N7 NK cells. The node for trajectory dominated by pre-infusion cells (pre-infusion trajectory) was centered on N1 NK cells as they are observed across all products. N7 cells formed their own trajectory un-attached to all other cells and were thus excluded from pseudotime computation.

High N5 and low N5 cells were defined as the top and bottom 30^{th} percentile of cells in N5 ordered by pseudotime. Differential expression was performed using the seurat function *FindMarkers*, differentially expressed genes were identified at adjusted P values < 0.1 and absolute log2 fold change > 1. Over-representation of hallmark pathways in up and down regulated genes were respectively computed using clusterprofiler (*38*); pathways were identified at $p < 0.05$ and $q < 0.1$.

Analysis of pathway activity in NK cells and tumor cells

Hallmark pathway activity of single cells was quantified from normalized gene expression levels using single-sample gene set enrichment analysis (ssGSEA) implemented in GSVA (*19*). To compare pathway activity between groups of cells we used Wilcoxon rank-sum test. In cases of multiple testing, the P values were corrected using FDR. While plotting heatmaps of differentially active pathways, pathways significantly different in at least one comparison were reported. A pathway was called differentially active in a comparison if $q < 0.01$ and the absolute difference in mean activity is greater than the 25^{th} percentile of all absolute differences in mean activity.

To quantify how pathway activity of cells in a cluster changes over time, we regressed pathway activity of the cells against time in weeks using linear regressions. Significance is determined at $p < 0.05$.

Heatmap in **fig. S6C** was generated by identifying differentially expressed genes (adjusted_p_value < 0.01 and absolute log2 fold change > 1), between tumor and NK cells using *FindMarkers* function in Seurat using the Wilcoxon rank-sum test. These genes were intersected with genes in 6 pathways of interest (OXPHOS, glycolysis, fatty acid metabolism, MYC targets V1, MYC targets V2 and MTORC1 signaling).

The scaled expression of these genes are Z-transformed and plotted as a heatmap using the R package *Pheatmap* (https://CRAN.R-project.org/package=pheatmap).

Gene set activity score calculation

We used the ssGSEA (*19*) method to calculate the metabolic pathway activity. Given a set of genes, a signature score was generated for each cell. The 85 metabolic pathways were extracted from the Kyoto Encyclopedia of Genes and Genomes (KEGG) (*39*). The KEGG metabolic pathways consist of amino-acid metabolism, carbohydrate metabolism, lipid metabolism, glycan metabolism, cofactor & vitamin metabolism, secondary metabolite metabolism, energy metabolism, other amino acid metabolism, and nucleotide xenobiotics metabolism. We added another two gene signatures related to mTOR, and glucose deprivation. The average metabolic activity for each cell was calculated by averaging the 87 metabolic pathway scores.

Glucose deprivation scores were calculated based on *NRN1*, *FAM129A*, *IL23A*, *SPRY1*, *GADD45B*, *HSPA1A*, *HSPA1B*, *GPNMB*, *HAVCR2*, *SOAT2*, and *ADAMTS6*. The mTOR pathway gene set was downloaded from BIOCARTA pathways version 7.0 (*40*). Activation scores were based on *CD244*, *CD226*, *KLRC2*, *KLRK1*, *NCR3*, *NCR1*, *NCR2*, *CD69*, *IL2RA*, *KIR2DS1*, KIR2DS2, *KIR2DS4*, *FCGR3A*, *LAMP1*, and *KIT*. Inhibition scores were based on *KIR2DL2*, *KIR2DL3*, *KLRD1*, *KLRC1*, *KIR3DL1*, *SIGLEC7*, *LAG3*, *HAVCR2*, *TIGIT*, *PDCD1*, and *LILRB*1. NK function scores were based on *TNFSF10*, *PRF1*, *SYK*, *ZAP70*, *GZMB*, *GZMA*, *FAS*, *CD247*, *GZMH*, and *GZMK*. The trend curves were generated using loess smoothing.

Patient scRNA-seq data analysis

UMAP analysis of patient scRNA-seq data

First, we reduced the dimensionality of the gene expression matrix using RunPCA in Seurat V3.0 (*33*), and the first 50 principal components were used as the inputs to UMAP generation. The UMAP plot was generated using the Seurat RunUMAP Implementation.

Identification of differentially expressed genes (DEGs)

The DEGs between different time points and patients were analyzed using Seurat. We used the MAST test (*41*) in the Findmarkers function to perform DE analysis. We then ranked genes by the log2 fold change and extracted the top 15 and bottom 15 genes. The heatmap of extracted genes were generated using the R package ComplexHeatmap (*34*).

Functional analysis and gene set enrichment analysis (GSEA)

We performed GSEA to identify differentially activated and suppressed pathways between two transcriptomes using the clusterProfiler package (*42*). Genes were ranked based on log2 fold change of relative expression levels. Only the pathways with FDR-adjusted P values less than 0.05 were shown in the dot plot using the Seurat Dotplot function.

Cell type annotation

We performed manual cell type annotation based on marker gene expression, and then automatic cell type labeling was performed for confirmation. Tumor B cells were defined as the cluster having expression of *CD19*, *MS4A1*(CD20), or *BCL2*. NK cells were defined as the cluster with a marker expression of *NCAM1*(CD56), *NKG7,* and *FCGR3A* (CD16). Other immune cell type markers were also screened. The automatic cell-type annotation of patient single-cell sequencing data was performed by SingleR package (*43*). We ran singleR against the reference HumanPrimaryCellAtlasData from the celldex package (*44*) and label.main was used for cell-type assignments.

Mass cytometry data analysis

Mass cytometry data pre-processing

Sample processing, antibody conjugation and sample staining were performed as previously described (*45*). Raw mass cytometry data were extracted into FCS files using CyTOF instrument (Helios). Single cells were gated using FlowJo software on the basis of event length and cell ID. In experiments focusing on NK cells, we also excluded events that were CD3+. Data from 36 samples were merged together using the R package cytofkit (*46*) on 33 surface markers. The transformation using *arcsinh* with a cofactor of 5 were performed to facilitate comparison between samples. For each surface marker, the maximum intensity observed over the 99.5^{th} percentile across all samples was excluded to exclude high-intensity outliers. Data from all samples were divided by these maximum values. As a result, intensity values for each marker ranged from 0 to 1. Unsupervised clustering was performed on the aggregated population of cells using "*PhenoGraph*" function in cytofkit (*46*) with the number of nearest neighbors being 30. Subsequently, tSNE plot was generated for cluster visualization. **Table S3** summarized the antibodies used to characterize the heterogeneity of CAR-NK cells and their phenotypical evolution over time. **Table S4** was generated to profile NK cells from two donors with different HLA types (donor #1-HLA-A3 and donor #2-HLA-A2) and to allow the simultaneous phenotypic characterization of NK cells from both donors across the duration of the experiments (**Fig. 6**).

Single-cell trajectory reconstruction from mass cytometry data

Cell fate decisions and differentiation trajectories were reconstructed with the Monocle v2 package (*17*) on the mass cytometry data of NK cells. To reduce computational time, trajectory analysis was performed based on randomly down-sampled data, consisting of 250 cells in each organ at each timepoint to ameliorate data-imbalance caused by large differences in numbers of cells in each sample. The set of 33 surface protein markers was used to order cells along a trajectory. The '*tobit*' expression family and '*DDRTree*' reduction method were used under the default parameters. Cells ordered in the pseudotime were clustered into distinct states.

Statistical analyses

Comparison between two groups was performed using two-tailed unpaired Student's *t* test or Mann–Whitney two-tailed test, with P value < 0.05 being statistically significant. All graphs show the mean $\pm$ s.e.m. unless otherwise indicated. GraphPad Prism 8 was used for statistical analysis of the experiments, data processing and presentation.

Supplementary Figures

Fig. S1

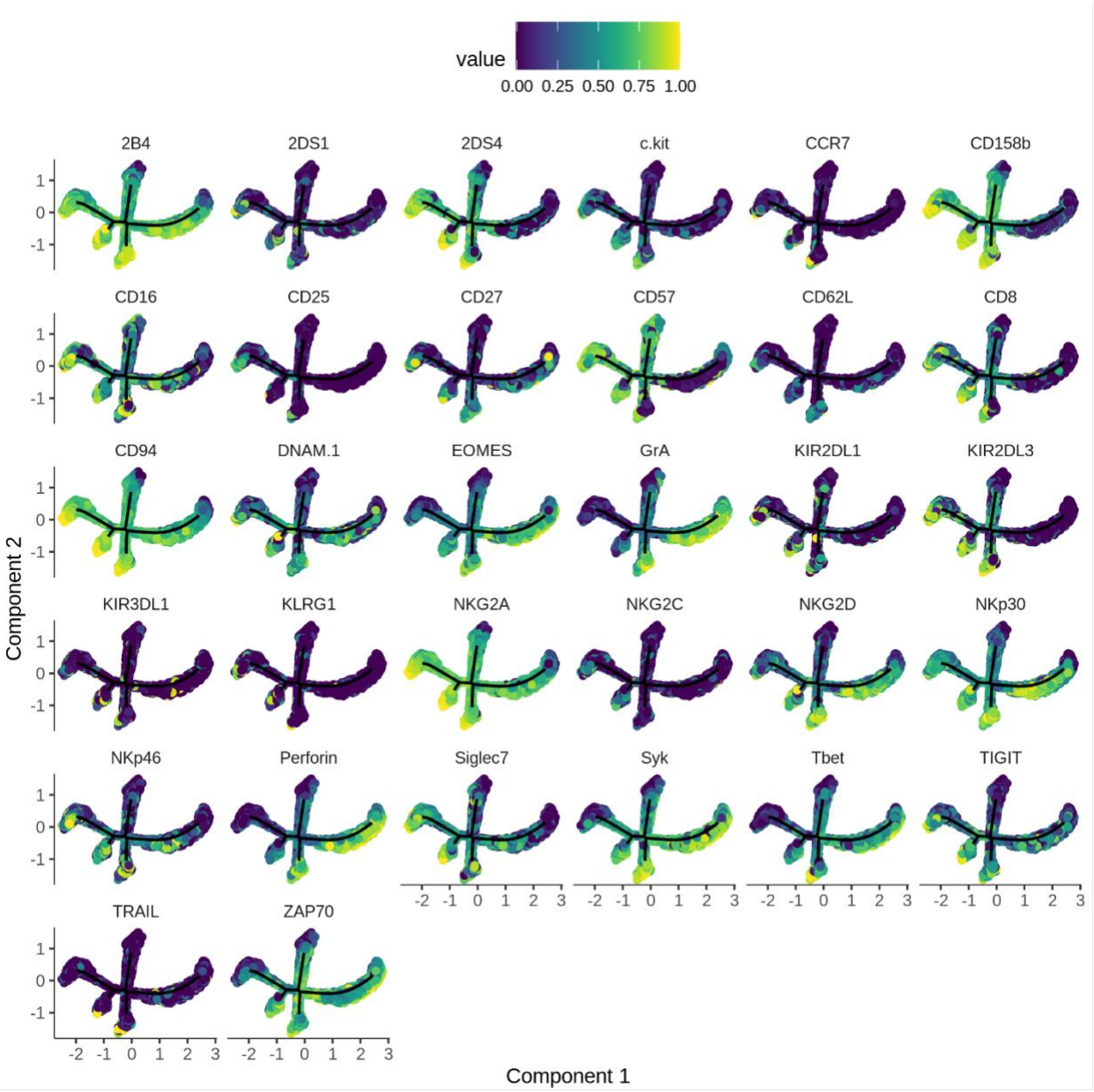

Fig. S1. Protein expression on trajectory analysis (related to Fig. 2F). Individual maps showing the expression of 32 human NK cell markers for NT, CAR19 and CAR19/IL-15 NK cells collected from mice at different time points as determined by mass cytometry. Color scale indicates the signal intensity, ranging from low (dark green) to high (yellow) after arcsine transformation.

Fig. S2

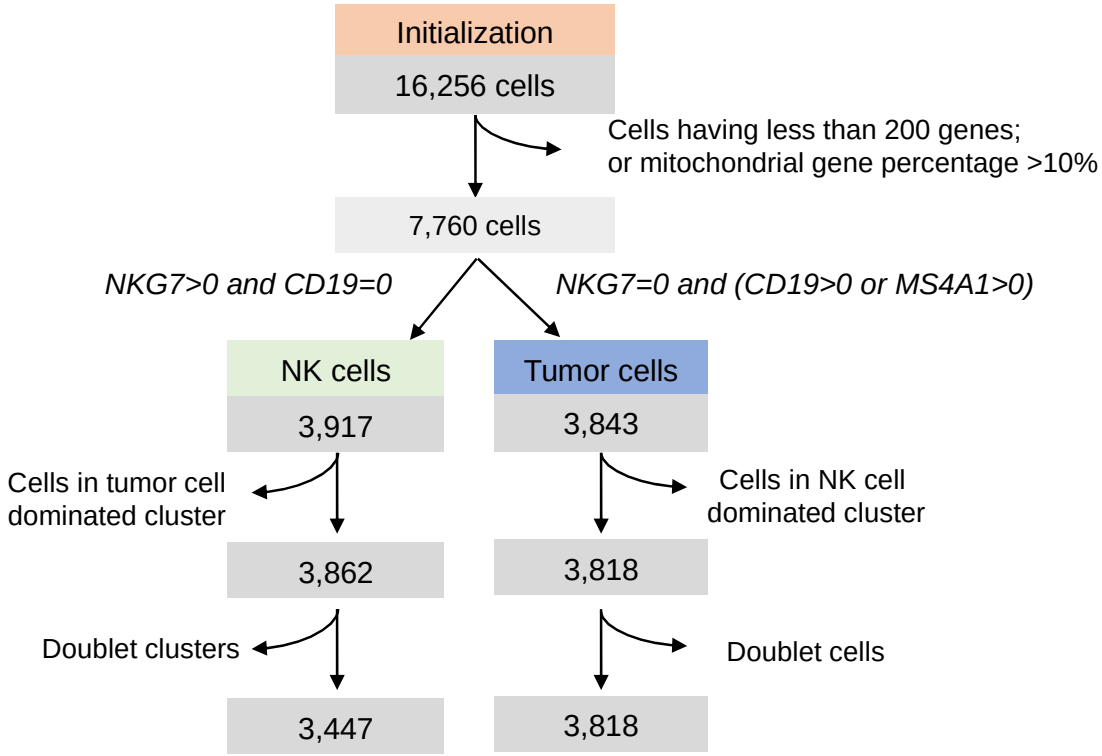

Fig. S2. Single cell RNA sequencing quality control process. Schematic outlining the different criteria applied to data quality control assessment during pre-processing of scRNA-seq.

Fig. S3

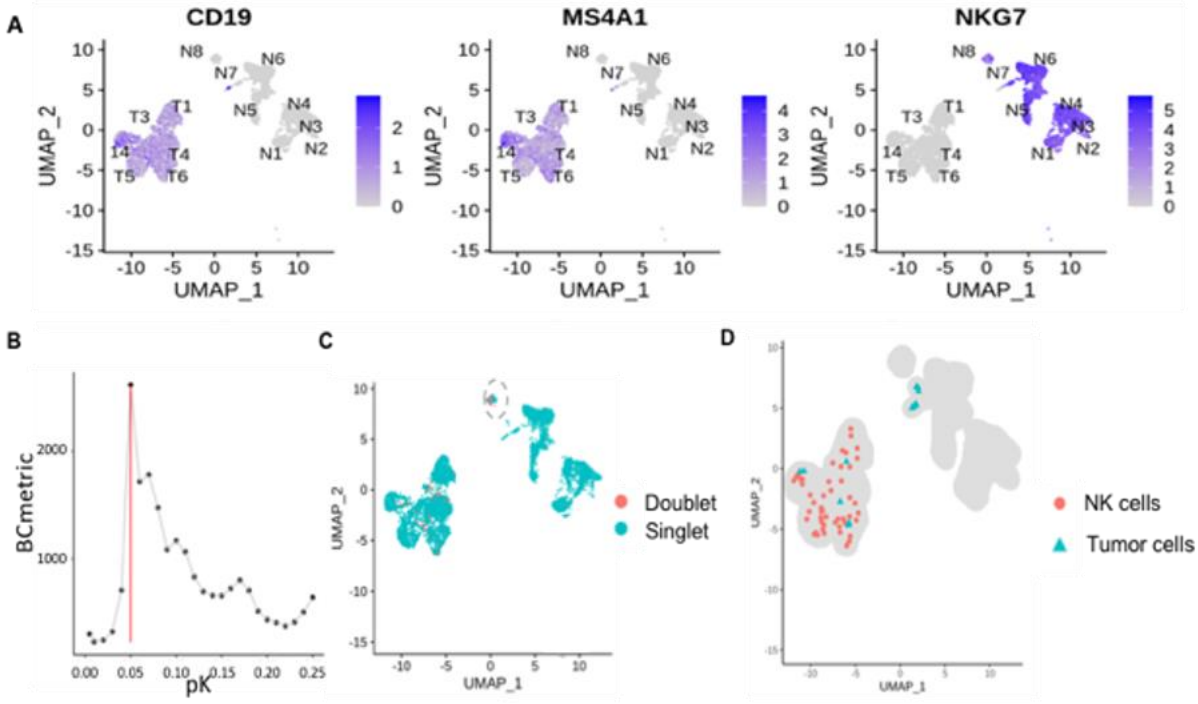

Fig. S3. Single cell RNA-seq data processing. (**A**) UMAP plot showing gene expression levels of *CD19* and *MS4A1* for tumor cells and *NKG7* for NK cells. Color scale indicates the signal intensity, ranging from low (grey) to high (blue). The NK cell cluster N8 was removed from downstream analysis as part of quality control data processing as they represented doublets. (**B**) BC_{MVN} distributions inform pK parameter selection for DoubletFinder software. BC_{MVN}: mean-variance-normalized bimodality coefficient. pK: Neighborhood size used to compute the number of artificial nearest neighbors. Red line denotes optimal pK value based on peak BC_{MVN}. (**C**) UMAP visualization of predicted doublets (red) and singlets (green) highlighting 2 putative doublet that were removed prior to downstream analysis. (**D**) UMAP visualization of tumor cells (green triangles) located in NK cells dominated clusters and NK cells (red circles) located in tumor cells dominated clusters. These were also removed as part of data quality control processing.

Fig. S4

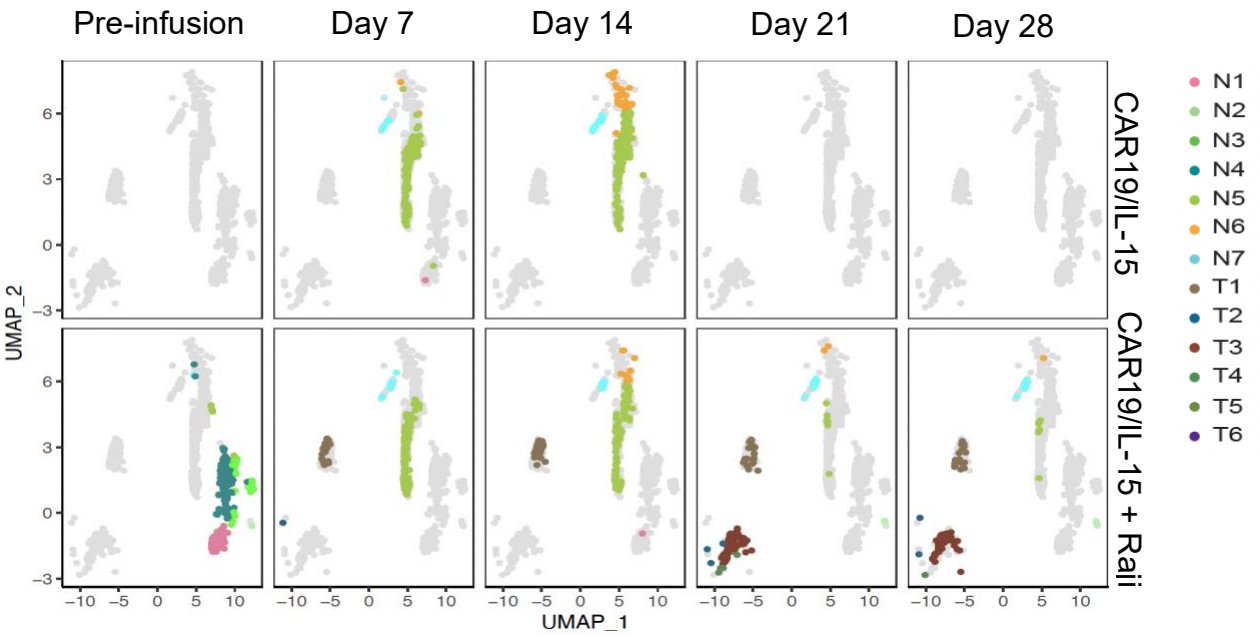

Fig. S4. CAR19/IL-15 NK cells require the presence of tumor cells for prolonged persistence. UMAP plot from scRNA-seq data showing the transcriptomic clusters of NK cells (N1-N7) and the Raji tumor cells (T1-T6) in mice receiving CAR19/IL-15 cells without Raji (top) or CAR19/IL-15 with Raji (bottom) and how they evolve and persist over time from pre-infusion (day 0) to day 28 after infusion.

Fig. S5

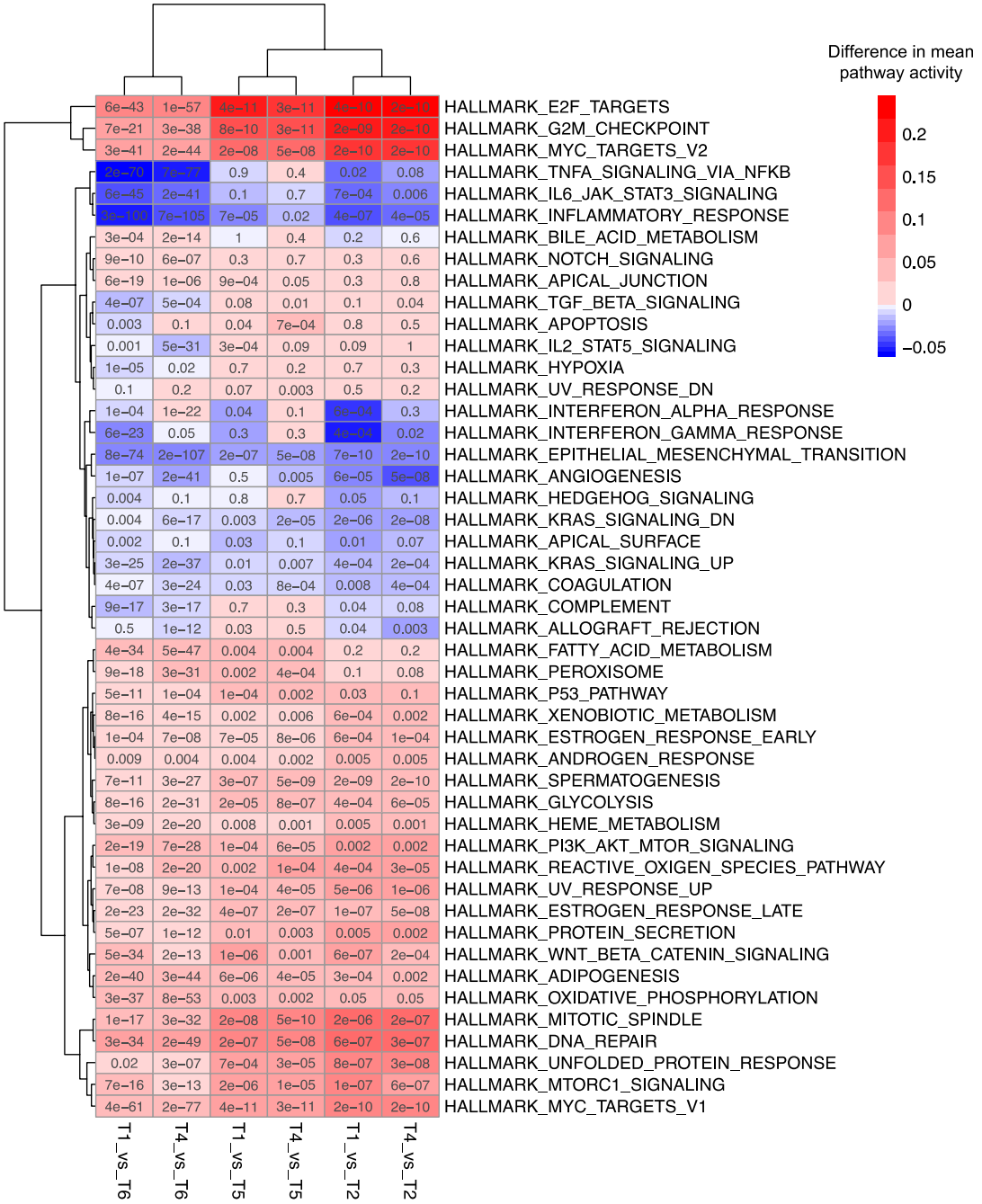

Fig. S5. **Differential pathway analysis between NK-sensitive and NK-resistant tumor clusters.** Heatmap of difference in mean pathway activity between tumor cells in indicated tumor clusters (T1-T6). Differential pathway activity in each comparison was inferred using Wilcox test, P values were corrected by FDR. The digits reported in the cells are the corresponding q-values. Only pathways significantly dysregulated ($q < 0.01$ and absolute difference in mean pathway activity > 25^{th} percentile of all absolute differences) in at least one of the comparisons is reported in the heatmap.

Fig. S6

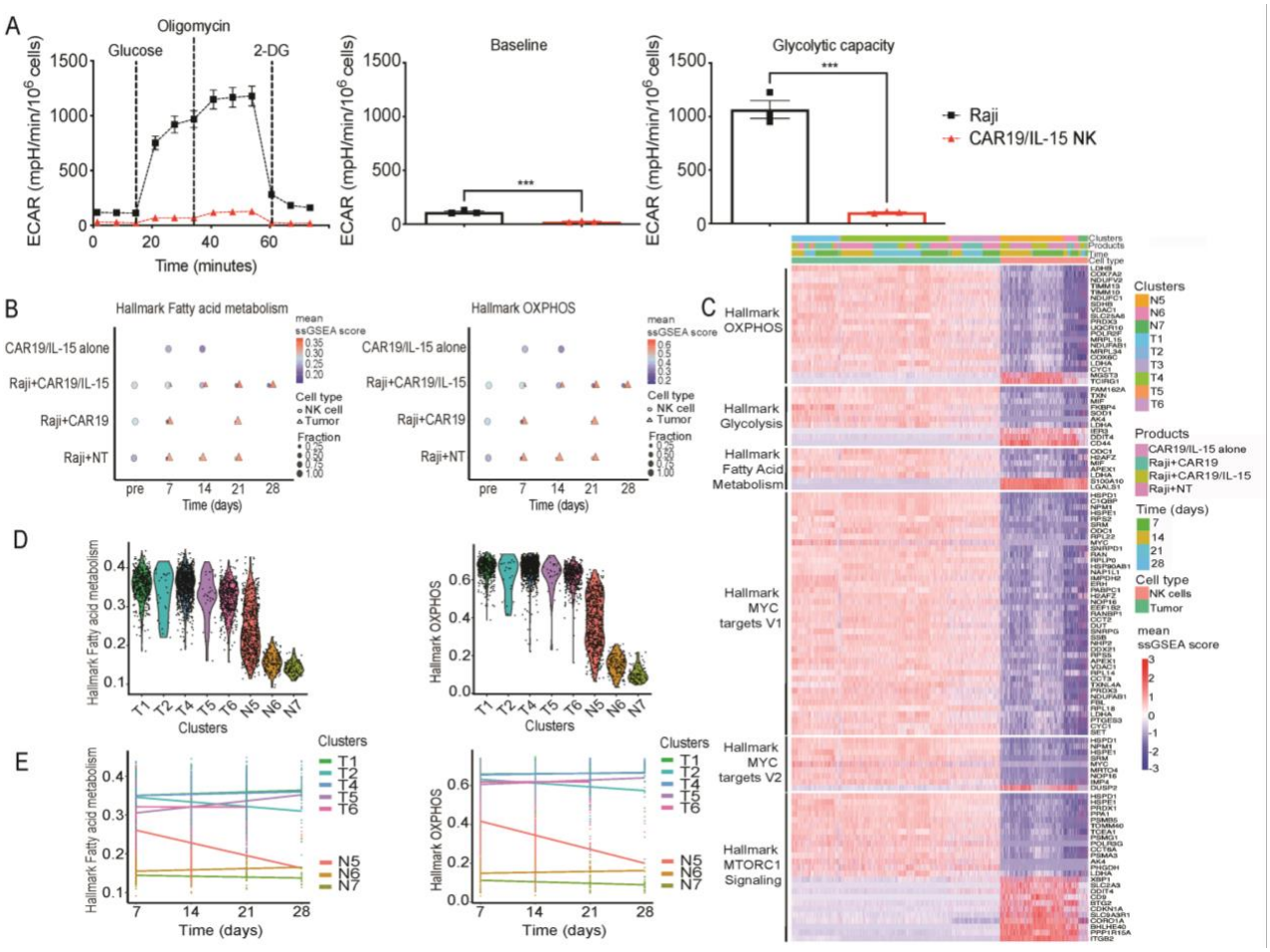

Fig. S6. Metabolic activity of NK cell (N5-N7) and tumor cell (T1-T6) clusters. (**A**) Extracellular acidification rate (ECAR) measured by Seahorse assays from CAR19/IL-15 NK (dashed red line) and Raji (dashed black lines) cells (left). Bar graphs show the basal ECAR (center), and the glycolytic capacity (right) of Raji and CAR19/IL-15 NK cells. The error bars represent the standard error of the mean estimated from triplicates. ***p ≤ 0.01. P values were determined by paired t-test. (**B**) Dot plots comparing the activity of fatty acid metabolism (left) and OXPHOS (right) pathways for tumor (triangle) and NK cells (circle) in each product (NT, CAR19, and CAR19/IL-15 NK) at pre-infusion (pre, day 0), and at days 7, 14, 21, and 28 post-NK infusion. The pathway activity of NK and tumor cells for each product at each time point with available data were compared with a Wilcox test and all P values corrected using FDR. The color of the dot indicates the mean pathway activity and the size the proportion of cells. (**C**) Heatmap of differentially expressed genes (q< 0.01 and absolute log2FC > 1) in post-infusion NK cell clusters (N5-N7) from the products NT, CAR19, and CAR19/IL-15 NK relative to Raji tumor cell clusters (T1-T6) in selected pathways of interest. (**D**) Violin plot of fatty acid metabolism (left) and OXPHOS (right) pathway activity across tumor (T1-T6) and NK cell clusters (N5-N7). **E**, Line plot of fatty acid metabolism (left) and OXPHOS (right) pathway activity across tumor (T1-T6) and NK cell clusters (N5-N7) at days 7, 14, 21, and 28 post-infusion.

Fig. S7

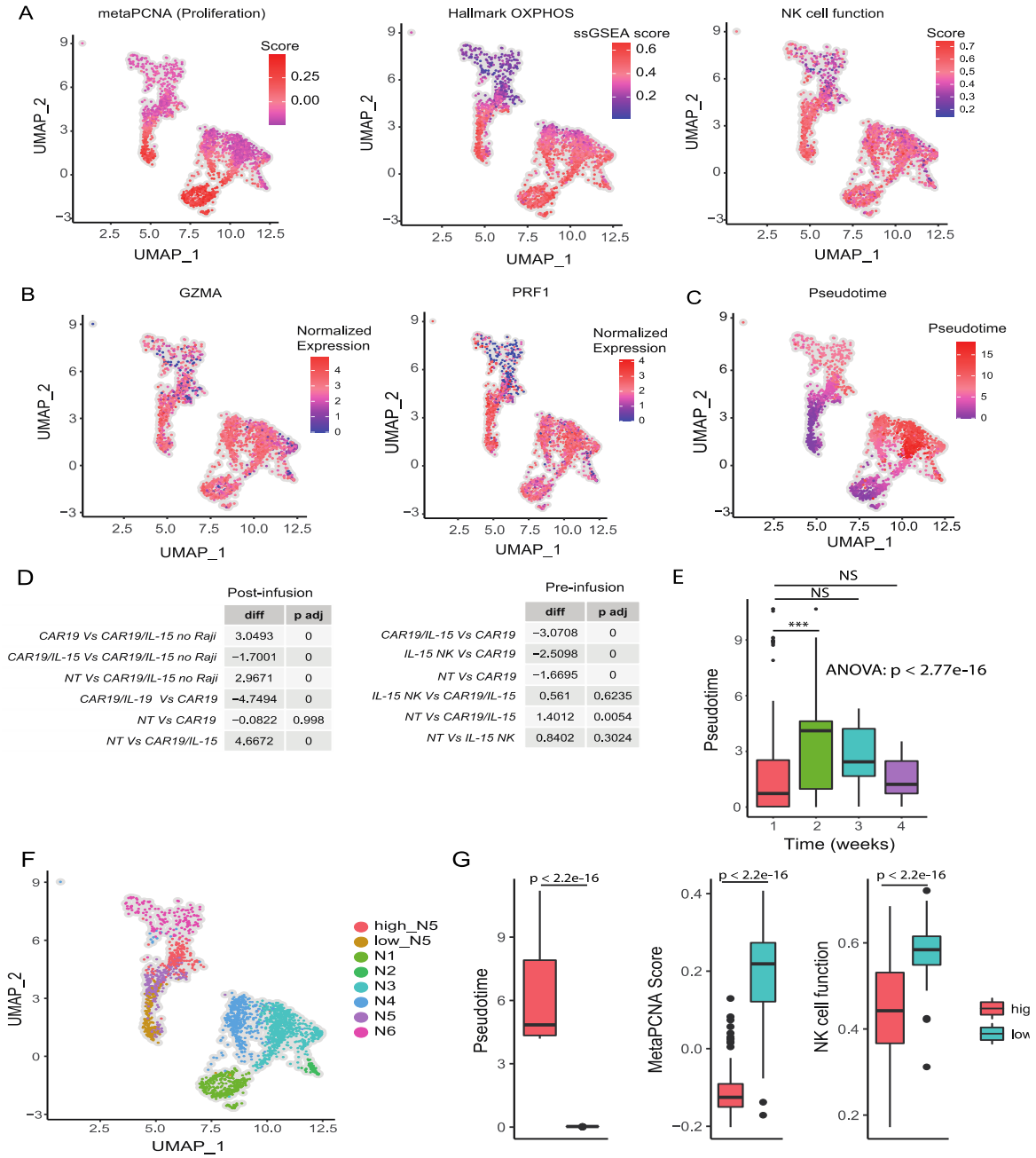

Fig. S7. Heterogeneity of NK cells clusters. (**A**) Functional indicators of NK cell clusters in pre- and post-treatment trajectories from Fig. 5A (metaPCNA proliferation score, hallmark OXPHOS pathway score and NK cell function score). (**B**) Normalized expression of NK cell effector genes *PRF1* and *GZMA* and (**C**) pseudotime. (**D**) Posthoc Tukey's pairwise testing comparing pseudotime of Fig 5D. (**E**) Pseudotime of N5 cells compared across experimental time in weeks; statistical testing of difference in means was performed using ANOVA and Tukey's posthoc test (adjusted P values: *** < 0.01, NS > 0.1). (**F**) UMAP depicting low N5 and high N5 cells. (**G**) Boxplots comparing pseudotime, proliferation (metaPCNA score) and NK cell function score between low and high N5 cells. P values reported are computed using Wilcox test.

Fig. S8

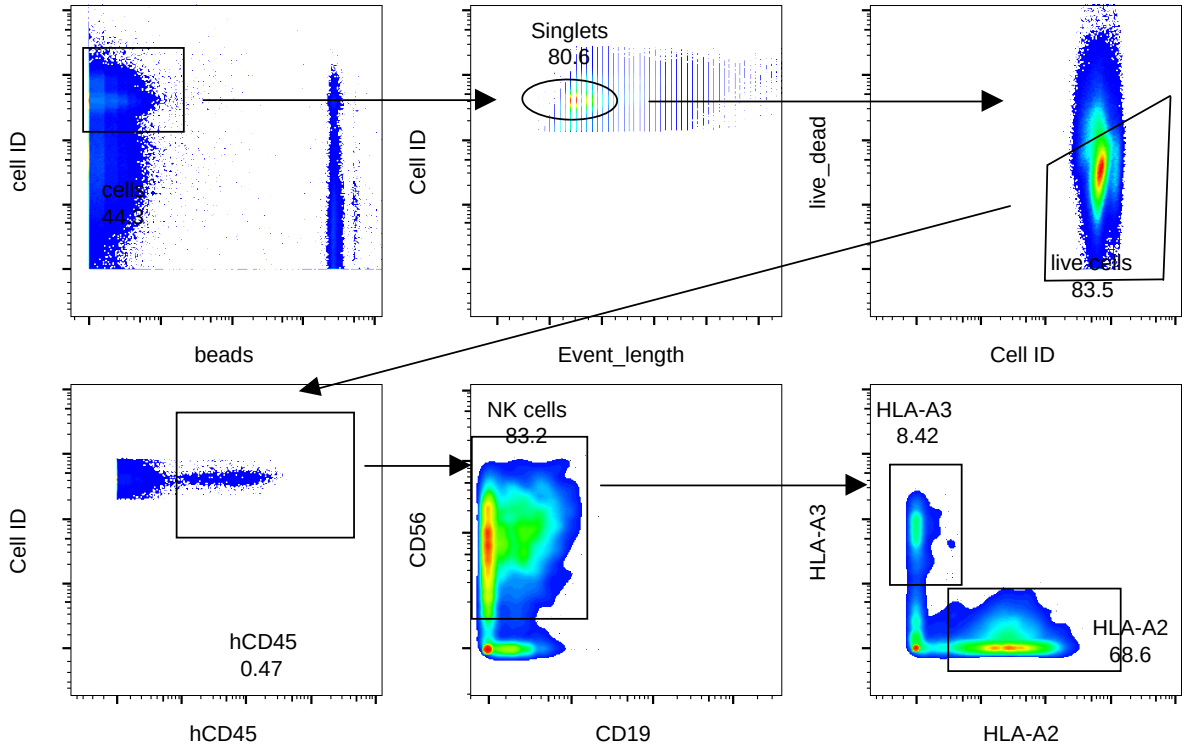

Fig. S8. Gating strategy to identify NK cells from donor #1 (HLA-A3 positive) and donor #2 (HLA-A2 positive). Representative mass cytometry plots showing gating strategy to identify NK cell from donor #1 and from donor #2. Briefly, 140Ce_calibration beads and 191Ir_cell ID were used to gate on cells; next doublets were excluded using Event_Length and live cells were selected using Live/Dead dye. Human NK cells were gated on hCD45+ CD56+ and then the donors were identified based on their HLA type (HLA-A3-donor #1 and HLA-A2-donor #2).

Fig. S9

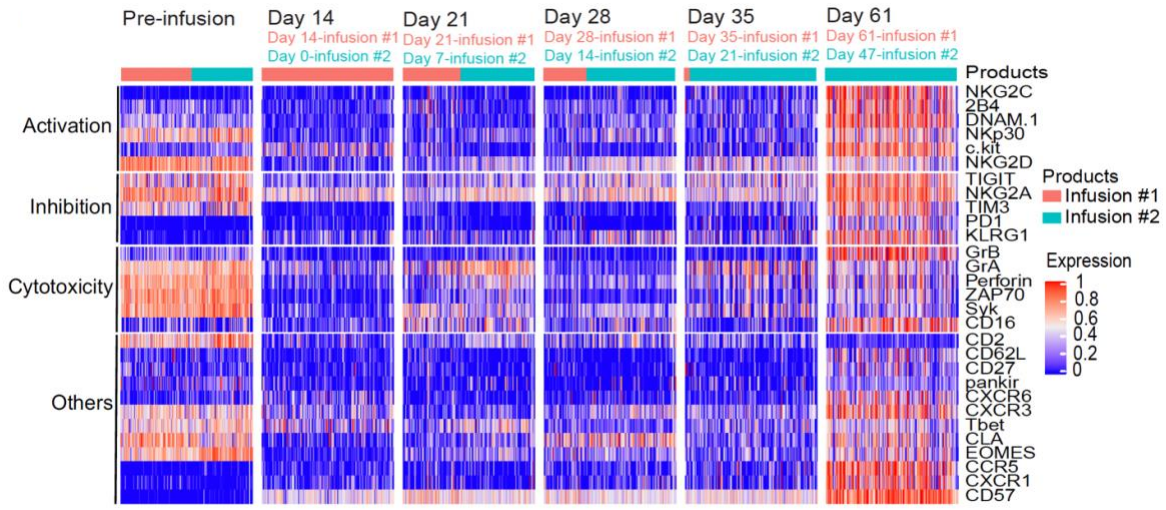

Fig. S9. Phenotype of CAR-NK cells derived from the two infusions. Heatmap showing the mass cytometry proteomic marker level of the first and the second infusions at different timepoints. Columns correspond to cells grouped by the infusion products and timepoints. Each row shows the mean level of a marker normalized over columns to a range of 0.2 (blue) and 1 (red).

Fig. S10

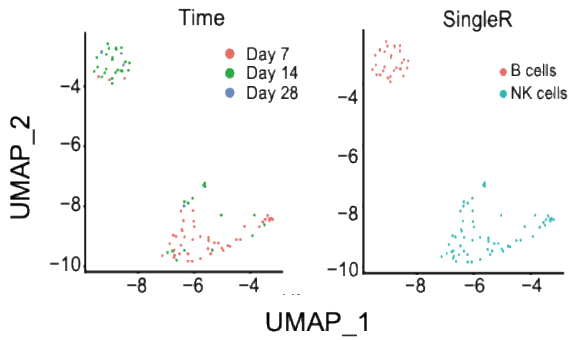

Fig. S10. Transcriptomic profiling of two patients treated with CAR19/IL-15 immunotherapy. UMAP plots of patient 6 and patient 10 single-cell sequencing data showing the distribution of two clusters colored by time (left) and SingleR cell-type labeling (right).

Supplementary Tables

Table S1. Number of cells for each product at every timepoint for scRNA-seq data.

NK cells					
Group	Pre-infusion (NK only)	Day 7	Day 14	Day 21	Day 28
Raji+NT NK	229	42	30	17	0
Raji+IL-15 NK	165	N/A	0	0	0
Raji+CAR19 NK	948*	50	N/A	30	0
Raji+CAR19/IL-15 NK	271#	160	113	35	33
CAR19/IL-15 NK alone (no Raji)	#	163	258	0	0
Tumor cells					
Group	Pre-infusion	Day 7	Day 14	Day 21	Day 28
Raji+NT-NK	0	402	505	118	0
Raji+IL-15 NK	0	0	0	0	0
Raji+CAR19 NK	0	260	0	512	0
Raji+CAR19/IL-15 NK	0	28	59	109	81

There are 18 groups that had NK cells detected. Note that no tumor cells are included for the Pre-infusion analysis.
# Indicates that the same CAR19/IL-15 NK cell product was infused into mice either alone (without co-administration of tumor) or with Raji tumor.
Zero (0) indicates that data were collected for this treatment, but no cells were detected.

Table S2. Statistical analysis of the stacked columns comparing the percentage of Raji and NK cells over time of mice receiving NT, CAR19 or CAR19/IL-15 NK cells (Fig. 2B).

Comparisons	Day 7 P value (0.0022)	Day 14 P value (7.82e-07)	Day 21 P value (2.6e-14)
NT vs CAR19	0.0123067 (20.975)	0.0000019 (81.368)	0.007245273 (4.9)
NT vs CAR19/IL-15	0.0018833 (28.925)	0.0000020 (85.250)	5.449526e-10 (99.9375)
CAR19 vs CAR19/IL-15	0.3120159 (-7.950)	0.8619972 (-3.882)	5.449540e-10 (-95.0375)

Differences in means were tested using ANOVA at each time point and reported in parenthesis in the corresponding column. Pairwise comparisons at each time point were tested using Tukey's test and the adjusted P values are reported in the table, with the difference between means of the two groups reported in parenthesis.

Table S3. List of antibodies used for 34-parameter mass cytometry panel to characterize the *in vivo* heterogeneity of NK cells and their phenotypical evolution over time.

Tag	Antibody	Clone	Source
141Pr	CD8	OKT8	Thermo Fisher
142Nd	CD94	DX22	Biolegend
143Nd	CD62L	DREG-56	BD Biosciences
144Nd	CD27	M-T271	Biolegend
145Nd	KIR2DS1	1127B	R&D
146Nd	CD56	HCD56	Biolegend
147Sm	NKG2C	134591	R&D
148Nd	KIR2DL2/L3(CD158B)	CH-L	BD Biosciences
149Sm	KIR2DS4	FES172	Beckman Coulter
151Eu	T-bet	4B10	Biolengend
152Sm	TIGIT	MBSA43	Thermo Fisher
153Eu	Siglec7	194211	R&D
154Sm	Granzyme A	CB9	Biolegend
155Gd	NKG2A	Z199	Beckman Coulter
156Gd	KIR2DL3	180701	R&D
158Gd	2B4	2-69	Biolegend
160Gd	TRAIL	RIK-2	Biolegend
161Dy	DNAM-1	DX11	Miltenyi
162Dy	Eomes	WD1928	Thermo Fisher
163Dy	NKp30	P30-15	Biolegend
164Dy	Ckit	2B8	BD Biosciences
165Ho	CD25	2A3	BD Biosciences
166Er	NKG2D	1D11	R&D
167Er	Perforin	B-D48	Abcam
168Er	ZAP70	1E7.2	Thermo Fisher
169Tm	KIR2DL1	143211	R&D
170Er	CD3	HIT3a	Bioledend
171Yb	CCR7	G043H7	Bioledend
172Yb	KIR3DL1	DX9	R&D
174Yb	Syk	4D10.2	Bioledend
175Lu	NKp46	195314	R&D
176Yb	KLRG1	13F12F2	Thermo Fisher
194Pt	CD57	HCD57	Biolegend
209Bi	CD16	3G8	Fluidigm

Table S4. List of antibodies used for 34-parameter mass cytometry panel to characterize the NK cells from two donors with different HLA types (donor #1 (HLA-A3+) vs donor #2 (HLA-A2+) from Figure 6.

Tag	Antibody	Clone	Source
89	hCD45	HI30	Biolegend
141Pr	CD2	TS1/8	Biolegend
142Nd	HLA-A3	GAP.A3	BD Pharmingen
143Nd	CD62L	DREG-56	BD Biosciences
144Nd	CD27	M-T271	Biolegend
145Nd	PanKIR	NKVFS1	Miltenyi
146Nd	CD56	HCD56	Biolegend
147Sm	NKG2C	134591	R&D
148Nd	CXCR6	CH-L	BD Biosciences
149Sm	CXCR3	FES172	Beckman Coulter
150Nd	Granzyme B	GB11	BD Biosciences
151Eu	Tbet	4B10	Biolengend
152Sm	TIGIT	MBSA43	Thermo Fisher
153Eu	HLA-A2	BB7.2	BD Pharmingen
154Sm	Granzyme A	CB9	Biolegend
155Gd	NKG2A	Z199	Beckman Coulter
156Gd	TIM3	F38-2E2	Biolegend
158Gd	2B4	2-69	Biolegend
160Gd	CD20	RIK-2	Biolegend
161Dy	DNAM-1	DX11	Miltenyi
162Dy	Eomes	WD1928	Thermo Fisher
163Dy	NKp30	P30-15	Biolegend
164Dy	Ckit	2B8	BD Biosciences
166Er	NKG2D	1D11	R&D
167Er	Perforin	B-D48	Abcam
168Er	ZAP70	1E7.2	Thomo Fisher
169Tm	CCR5	J418F1	Biolegend
170Er	CAR	Polyclonal	Jackson immune research
172Yb	CXCR1	8f1/ccxcr1	Biolegend
173Yb	PD1	EH12.2H7	Biolegend
174Yb	Syk	4D10.2	Bioledend
176Yb	KLRG1	13F12F2	Thermo Fisher
194Pt	CD57	HCD57	Biolegend
209Bi	CLA	HECA-452	Biolegend

Table S5. Number of cells for each patient at every timepoint for scRNA-seq data after processing and quality control.

Patient	**Cell type**	**Time (days)**	**Total number of cells**
Patient 6	NK cell	Day 7	35
Patient 6	NK cell	Day 14	8
Patient 10	B cell	Day 7	3
Patient 10	B cell	Day 14	24
Patient 10	B cell	Day 28	3
Patient 10	NK cell	Day 7	9
Patient 10	NK cell	Day 14	7
Patient 10	NK cell	Day 28	1

Table S6. Statistical analysis of the dot plots comparing the metabolic activity of glycolysis (Fig. 4B), fatty acid metabolism and OXPHOS (fig. S6B).

Glycolysis			
T vs NK Comparisons	Mean difference	P value	q
Raji+NT NK_D7	0.138019	2.09E-27	9.41E-27
Raji+NT NK_D14	0.068715	4.29E-12	5.51E-12
Raji+NT NK_D21	0.070006	2.79E-06	2.79E-06
Raji+CAR19 NK_D7	0.138617	2.03E-30	1.83E-29
Raji+CAR19 NK_D21	0.117724	3.17E-18	5.7E-18
Raji+CAR19/IL-15 NK_D7	0.052306	5.81E-07	6.53E-07
Raji+ CAR19/IL-15 NK_D14	0.102606	2.51E-22	7.54E-22
Raji+ CAR19/IL-15 NK_D21	0.152343	1.51E-18	3.4E-18
Raji+ CAR19/IL-15 NK_D28	0.147417	5.07E-16	7.59E-16
OXPHOS			
T vs NK Comparisons	Mean difference	P value	q
Raji+NT NK_D7	0.48246	1.71E-27	7.69E-27
Raji+NT NK_D14	0.233414	2.44E-18	3.65E-18
Raji+NT NK_D21	0.247591	3.23E-09	3.23E-09
Raji+CAR19 NK_D7	0.47225	3.81E-32	3.42E-31
Raji+ CAR19 NK_D21	0.397818	3.40E-19	7.66E-19
Raji+CAR19/IL-15 NK_D7	0.187441	1.57E-12	1.76E-12
Raji+ CAR19/IL-15 NK_D14	0.339641	1.45E-26	4.36E-26
Raji+ CAR19/IL-15 NK_D21	0.475875	1.08E-18	1.95E-18
Raji+ CAR19/IL-15 NK_D28	0.491316	2.46E-16	3.15E-16
Fatty acid metabolism			
T vs NK Comparisons	Mean difference	P value	q
Raji+NT NK_D7	0.176309	1.47E-26	6.622E-26
Raji+NT NK_D14	0.076132	1.70E-09	2.187E-09
Raji+NT NK_D21	0.077143	0.000337	0.00036874
Raji+CAR19 NK_D7	0.18097	1.78E-29	1.6E-28
Raji+ CAR19 NK_D21	0.140338	8.41E-15	1.26E-14
Raji+CAR19/IL-15 NK_D7	0.062341	1.13E-05	1.26E-05
Raji+ CAR19/IL-15 NK_D14	0.134084	7.11E-22	2.131E-21
Raji+ CAR19/IL-15 NK_D21	0.192947	8.12E-18	1.82E-17
Raji+ CAR19/IL-15 NK_D28	0.193144	6.01E-15	1.08E-14

Table S7. Linear regression analysis for glycolysis (Fig. 4D), fatty acid metabolism and OXPHOS (fig. S6E) between post-infusion NK cell clusters (N5, N6, N7) and tumor clusters (T1-T6).

Cluster	Glycolysis slope	Glycolysis P value	Fatty acid metabolism slope	Fatty acid metabolism P value	OXPHOS slope	OXPHOS P Value
N5	-0.021833	3.36E-12	-0.032582	1.04E-12	-0.072118	3.04E-14
N6	8.18E-05	0.969067	0.003368	0.168768	0.004474	0.397284
N7	-0.000505	0.673284	-0.002298	0.117873	-0.007768	0.023086
T1	0.003617	0.025704	0.004443	0.025364	0.002035	0.432325
T2	-0.006439	0.414371	-0.011910	0.284235	-0.019263	0.296968
T4	0.002458	0.014484	0.003275	0.012650	0.004062	0.027763
T5	0.002513	0.723527	0.015486	0.178665	0.011182	0.550459
T6	-0.000214	0.897072	-0.000457	0.833821	0.000179	0.951978

REFERENCES AND NOTES

1. S. S. Neelapu, F. L. Locke, N. L. Bartlett, L. J. Lekakis, D. B. Miklos, C. A. Jacobson, I. Braunschweig, O. O. Oluwole, T. Siddiqi, Y. Lin, J. M. Timmerman, P. J. Stiff, J. W. Friedberg, I. W. Flinn, A. Goy, B. T. Hill, M. R. Smith, A. Deol, U. Farooq, P. McSweeney, J. Munoz, I. Avivi, J. E. Castro, J. R. Westin, J. C. Chavez, A. Ghobadi, K. V. Komanduri, R. Levy, E. D. Jacobsen, T. E. Witzig, P. Reagan, A. Bot, J. Rossi, L. Navale, Y. Jiang, J. Aycock, M. Elias, D. Chang, J. Wiezorek, W. Y. Go, Axicabtagene ciloleucel CAR T-cell therapy in refractory large B-cell lymphoma. *N. Engl. J. Med.* **377**, 2531–2544 (2017).

2. S. J. Schuster, M. R. Bishop, C. S. Tam, E. K. Waller, P. Borchmann, J. P. McGuirk, U. Jäger, S. Jaglowski, C. Andreadis, J. R. Westin, I. Fleury, V. Bachanova, S. R. Foley, P. J. Ho, S. Mielke, J. M. Magenau, H. Holte, S. Pantano, L. B. Pacaud, R. Awasthi, J. Chu, Ö. Anak, G. Salles, R. T. Maziarz, Tisagenlecleucel in adult relapsed or refractory diffuse large B-cell lymphoma. *N. Engl. J. Med.* **380**, 45–56 (2019).

3. S. L. Maude, T. W. Laetsch, J. Buechner, S. Rives, M. Boyer, H. Bittencourt, P. Bader, M. R. Verneris, H. E. Stefanski, G. D. Myers, M. Qayed, B. de Moerloose, H. Hiramatsu, K. Schlis, K. L. Davis, P. L. Martin, E. R. Nemecek, G. A. Yanik, C. Peters, A. Baruchel, N. Boissel, F. Mechinaud, A. Balduzzi, J. Krueger, C. H. June, B. L. Levine, P. Wood, T. Taran, M. Leung, K. T. Mueller, Y. Zhang, K. Sen, D. Lebwohl, M. A. Pulsipher, S. A. Grupp, Tisagenlecleucel in children and young adults with B-cell lymphoblastic leukemia. *N. Engl. J. Med.* **378**, 439–448 (2018).

4. J. H. Park, I. Rivière, M. Gonen, X. Wang, B. Sénéchal, K. J. Curran, C. Sauter, Y. Wang, B. Santomasso, E. Mead, M. Roshal, P. Maslak, M. Davila, R. J. Brentjens, M. Sadelain, Long-term follow-up of CD19 CAR therapy in acute lymphoblastic leukemia. *N. Engl. J. Med.* **378**, 449–459 (2018).

5. D. L. Porter, B. L. Levine, M. Kalos, A. Bagg, C. H. June, Chimeric antigen receptor-modified T cells in chronic lymphoid leukemia. *N. Engl. J. Med.* **365**, 725–733 (2011).

6. N. C. Munshi, L. D. Anderson Jr, N. Shah, D. Madduri, J. Berdeja, S. Lonial, N. Raje, Y. Lin, D. Siegel, A. Oriol, P. Moreau, I. Yakoub-Agha, M. Delforge, M. Cavo, H. Einsele, H. Goldschmidt, K. Weisel, A.

Rambaldi, D. Reece, F. Petrocca, M. Massaro, J. N. Connarn, S. Kaiser, P. Patel, L. Huang, T. B. Campbell, K. Hege, J. San-Miguel, Idecabtagene vicleucel in relapsed and refractory multiple myeloma. *N. Engl. J. Med.* **384**, 705–716 (2021).

7. A. Mullard, FDA approves fourth CAR-T cell therapy. *Nat. Rev. Drug Discov.* **20**, 166 (2021).

8. S. S. Neelapu, S. Tummala, P. Kebriaei, W. Wierda, F. L. Locke, Y. Lin, N. Jain, N. Daver, A. M. Gulbis, S. Adkins, K. Rezvani, P. Hwu, E. J. Shpall, Toxicity management after chimeric antigen receptor T cell therapy: One size does not fit 'ALL'. *Nat. Rev. Clin. Oncol.* **15**, 218 (2018).

9. L. Chiossone, P. Y. Dumas, M. Vienne, E. Vivier, Natural killer cells and other innate lymphoid cells in cancer. *Nat. Rev. Immunol.* **18**, 671–688 (2018).

10. M. Daher, K. Rezvani, Outlook for new CAR-based therapies with a focus on CAR NK cells: What lies beyond CAR-engineered T cells in the race against cancer. *Cancer Discov.* **11**, 45–58 (2021).

11. E. Liu, D. Marin, P. Banerjee, H. A. Macapinlac, P. Thompson, R. Basar, L. Nassif Kerbauy, B. Overman, P. Thall, M. Kaplan, V. Nandivada, I. Kaur, A. Nunez Cortes, K. Cao, M. Daher, C. Hosing, E. N. Cohen, P. Kebriaei, R. Mehta, S. Neelapu, Y. Nieto, M. Wang, W. Wierda, M. Keating, R. Champlin, E. J. Shpall, K. Rezvani, Use of CAR-transduced natural killer cells in CD19-positive lymphoid tumors. *N. Engl. J. Med.* **382**, 545–553 (2020).

12. H. Klingemann, Are natural killer cells superior CAR drivers? *Onco. Targets Ther.* **3**, e28147 (2014).

13. E. J. Orlando, X. Han, C. Tribouley, P. A. Wood, R. J. Leary, M. Riester, J. E. Levine, M. Qayed, S. A. Grupp, M. Boyer, B. de Moerloose, E. R. Nemecek, H. Bittencourt, H. Hiramatsu, J. Buechner, S. M. Davies, M. R. Verneris, K. Nguyen, J. L. Brogdon, H. Bitter, M. Morrissey, P. Pierog, S. Pantano, J. A. Engelman, W. Winckler, Genetic mechanisms of target antigen loss in CAR19 therapy of acute lymphoblastic leukemia. *Nat. Med.* **24**, 1504–1506 (2018).

14. J. A. Fraietta, S. F. Lacey, E. J. Orlando, I. Pruteanu-Malinici, M. Gohil, S. Lundh, A. C. Boesteanu, Y. Wang, R. S. O'Connor, W.T. Hwang, E. Pequignot, D. E. Ambrose, C. Zhang, N. Wilcox, F. Bedoya, C. Dorfmeier, F. Chen, L. Tian, H. Parakandi, M. Gupta, R. M. Young, F. B. Johnson, I. Kulikovskaya, L. Liu, J. Xu, S. H. Kassim, M. M. Davis, B. L. Levine, N. V. Frey, D. L. Siegel, A. C. Huang, E. J.

Wherry, H. Bitter, J. L. Brogdon, D. L. Porter, C. H. June, J. J. Melenhorst, Determinants of response and resistance to CD19 chimeric antigen receptor (CAR) T cell therapy of chronic lymphocytic leukemia. *Nat. Med.* **24**, 563–571 (2018).

15. E. Liu, Y. Tong, G. Dotti, H. Shaim, B. Savoldo, M. Mukherjee, J. Orange, X. Wan, X. Lu, A. Reynolds, M. Gagea, P. Banerjee, R. Cai, M. H. Bdaiwi, R. Basar, M. Muftuoglu, L. Li, D. Marin, W. Wierda, M. Keating, R. Champlin, E. Shpall, K. Rezvani, Cord blood NK cells engineered to express IL-15 and a CD19-targeted CAR show long-term persistence and potent antitumor activity. *Leukemia* **32**, 520–531 (2018).

16. E. Becht, L. M. Innes, J. Healy, C.-A. Dutertre, I. W. H. Kwok, L. G. Ng, F. Ginhoux, E. W. Newell, Dimensionality reduction for visualizing single-cell data using UMAP. *Nat. Biotechnol.* **37**, 38–44 (2019).

17. C. Trapnell, D. Cacchiarelli, J. Grimsby, P. Pokharel, S. Li, M. Morse, N. J. Lennon, K. J. Livak, T. S. Mikkelsen, J. L. Rinn, The dynamics and regulators of cell fate decisions are revealed by pseudotemporal ordering of single cells. *Nat. Biotechnol.* **32**, 381–386 (2014).

18. K. Solocinski, M. R. Padget, K. P. Fabian, B. Wolfson, F. Cecchi, T. Hembrough, S. C. Benz, S. Rabizadeh, P. Soon-Shiong, J. Schlom, J. W. Hodge, Overcoming hypoxia-induced functional suppression of NK cells. *J. Immunother. Cancer* **8**, e000246 (2020).

19. S. Hänzelmann, R. Castelo, J. Guinney, GSVA: Gene set variation analysis for microarray and RNA-seq data. *BMC Bioinformatics* **14**, 7 (2013).

20. F. Rohrig, A. Schulze, The multifaceted roles of fatty acid synthesis in cancer. *Nat. Rev. Cancer* **16**, 732–749 (2016).

21. W. Li, M. Xu, Y. Li, Z. Huang, J. Zhou, Q. Zhao, K. le, F. Dong, C. Wan, P. Yi, Comprehensive analysis of the association between tumor glycolysis and immune/inflammation function in breast cancer. *J. Transl. Med.* **18**, 92 (2020).

22. X. Tang, L. Yang, Z. Li, A.P. Nalin, H. Dai, T. Xu, J. Yin, F. You, M. Zhu, W. Shen, G. Chen, X. Zhu, D. Wu, J. Yu, First-in-man clinical trial of CAR NK-92 cells: Safety test of CD33-CAR NK-92 cells in patients with relapsed and refractory acute myeloid leukemia. *Am. J. Cancer Res.* **8**, 1083–1089 (2018).

23. V. Bachanova, A. Ghobadi, K. Patel, J.H. Park, I.W. Flinn, P. Shah, C. Wong, C. Bickers, P. Szabo, L. Wong, B. Valamehr, S. Atwal, Y.W. Chu, R. Elstrom, P. Strati, Safety and efficacy of FT596, a first-in-class, multi-antigen targeted, off-the-shelf, iPSC-derived CD19 CAR NK cell therapy in relapsed/refractory B-cell lymphoma. *Blood* **138**, 823 (2021).

24. A. Marcais, J. Cherfils-Vicini, C. Viant, S. Degouve, S. Viel, A. Fenis, J. Rabilloud, K. Mayol, A. Tavares, J. Bienvenu, Y.-G. Gangloff, E. Gilson, E. Vivier, T. Walzer, The metabolic checkpoint kinase mTOR is essential for IL-15 signaling during the development and activation of NK cells. *Nat. Immunol.* **15**, 749–757 (2014).

25. C. Magaway, E. Kim, E. Jacinto, Targeting mTOR and metabolism in cancer: Lessons and innovations. *Cell* **8**, 1584 (2019).

26. A. H. Long, W. M. Haso, J. F. Shern, K. M. Wanhainen, M. Murgai, M. Ingaramo, J. P. Smith, A. J. Walker, M. E. Kohler, V. R. Venkateshwara, R. N. Kaplan, G. H. Patterson, T. J. Fry, R. J. Orentas, C. L. Mackall, 4-1BB costimulation ameliorates T cell exhaustion induced by tonic signaling of chimeric antigen receptors. *Nat. Med.* **21**, 581–590 (2015).

27. V. Hoyos, B. Savoldo, C. Quintarelli, A. Mahendravada, M. Zhang, J. Vera, H.E. Heslop, C.M. Rooney, M.K. Brenner, G. Dotti, Engineering CD19-specific T lymphocytes with interleukin-15 and a suicide gene to enhance their anti-lymphoma/leukemia effects and safety. *Leukemia* **24**, 1160–1170 (2010).

28. J. Vera, B. Savoldo, S. Vigouroux, E. Biagi, M. Pule, C. Rossig, J. Wu, H. E. Heslop, C. M. Rooney, M. K. Brenner, G. Dotti, T lymphocytes redirected against the κ light chain of human immunoglobulin efficiently kill mature B lymphocyte-derived malignant cells. *Blood* **108**, 3890–3897 (2006).

29. M. Daher, R. Basar, E. Gokdemir, N. Baran, N. Uprety, A. K. Nunez Cortes, M. Mendt, L. N. Kerbauy, P. P. Banerjee, M. Shanley, N. Imahashi, L. Li, F. L. W. I. Lim, M. Fathi, A. Rezvan, V. Mohanty, Y.

Shen, H. Shaim, J. Lu, G. Ozcan, E. Ensley, M. Kaplan, V. Nandivada, M. Bdiwi, S. Acharya, Y. Xi, X. Wan, D. Mak, E. Liu, X. R. Jiang, S. Ang, L. Muniz-Feliciano, Y. Li, J. Wang, S. Kordasti, N. Petrov, N. Varadarajan, D. Marin, L. Brunetti, R. J. Skinner, S. Lyu, L. Silva, R. Turk, M. S. Schubert, G. R. Rettig, M. S. McNeill, G. Kurgan, M. A. Behlke, H. Li, N. W. Fowlkes, K. Chen, M. Konopleva, R. E. Champlin, E. J. Shpall, K. Rezvani, Targeting a cytokine checkpoint enhances the fitness of armored cord blood CAR-NK cells. *Blood* **137**, 624–636 (2021).

30. E. Liu, S. O. T. Ang, L. Kerbauy, R. Basar, I. Kaur, M. Kaplan, L. Li, Y. Tong, M. Daher, E. L. Ensley, N. Uprety, A. K. Nunez Cortes, R. Z. Yang, Y. Li, H. Shaim, F. Reyes Silva, P. Lin, V. Mohanty, S. Acharya, M. Shanley, L. Muniz-Feliciano, P. P. Banerjee, K. Chen, R. E. Champlin, E. J. Shpall, K. Rezvani, GMP-compliant universal antigen presenting cells (uAPC) promote the metabolic fitness and antitumor activity of armored cord blood CAR-NK cells. *Front. Immunol.* **12**, 626098 (2021).

31. C. S. McGinnis, L. M. Murrow, Z. J. Gartner, DoubletFinder: Doublet detection in single-cell RNA sequencing data using artificial nearest neighbors. *Cell Syst.* **8**, 329–337. e324 (2019).

32. S. Picelli, O. R. Faridani, Å. K. Björklund, G. Winberg, S. Sagasser, R. Sandberg, Full-length RNA-seq from single cells using Smart-seq2. *Nat. Protoc.* **9**, 171–181 (2014).

33. T. Stuart, A. Butler, P. Hoffman, C. Hafemeister, E. Papalexi, W. M. Mauck, 3rd, Y. Hao, M. Stoeckius, P. Smibert, R. Satija, Comprehensive integration of single-cell data. *Cell* **177**, 1888–1902. e1821 (2019).

34. Z. Gu, R. Eils, M. Schlesner, Complex heatmaps reveal patterns and correlations in multidimensional genomic data. *Bioinformatics* **32**, 2847–2849 (2016).

35. M. V. Kuleshov, M. R. Jones, A. D. Rouillard, N. F. Fernandez, Q. Duan, Z. Wang, S. Koplev, S. L. Jenkins, K. M. Jagodnik, A. Lachmann, M. G. McDermott, C. D. Monteiro, G. W. Gundersen, A. Ma'ayan, Enrichr: A comprehensive gene set enrichment analysis web server 2016 update. *Nucleic Acids Res.* **44**, W90–W97 (2016).

36. D. Venet, J. E. Dumont, V. Detours, Most random gene expression signatures are significantly associated with breast cancer outcome. *PLOS Comput. Biol.* **7**, e1002240 (2011).

37. J. Cao, M. Spielmann, X. Qiu, X. Huang, D. M. Ibrahim, A. J. Hill, F. Zhang, S. Mundlos, L. Christiansen, F. J. Steemers, C. Trapnell, J. Shendure, The single-cell transcriptional landscape of mammalian organogenesis. *Nature* **566**, 496–502 (2019).

38. T. Wu, E. Hu, S. Xu, M. Chen, P. Guo, Z. Dai, T. Feng, L. Zhou, W. Tang, L. Zhan, X. Fu, S. Liu, X. Bo, G. Yu, clusterProfiler 4.0: A universal enrichment tool for interpreting omics data. *Innovation* **2**, 100141 (2021).

39. M. Kanehisa, S. Goto, KEGG: Kyoto encyclopedia of genes and genomes. *Nucleic Acids Res.* **28**, 27–30 (2000).

40. A. Subramanian, P. Tamayo, V. K. Mootha, S. Mukherjee, B. L. Ebert, M. A. Gillette, A. Paulovich, S. L. Pomeroy, T. R. Golub, E. S. Lander, J. P. Mesirov, Gene set enrichment analysis: A knowledge-based approach for interpreting genome-wide expression profiles. *Proc. Natl. Acad. Sci. U.S.A.* **102**, 15545–15550 (2005).

41. G. Finak, A. McDavid, M. Yajima, J. Deng, V. Gersuk, A. K. Shalek, C. K. Slichter, H. W. Miller, M. J. McElrath, M. Prlic, P. S. Linsley, R. Gottardo, MAST: A flexible statistical framework for assessing transcriptional changes and characterizing heterogeneity in single-cell RNA sequencing data. *Genome Biol.* **16**, 278 (2015).

42. G. Yu, L.-G. Wang, Y. Han, Q.-Y. He, clusterProfiler: An R package for comparing biological themes among gene clusters. *OMICS* **16**, 284–287 (2012).

43. D. Aran, A. P. Looney, L. Liu, E. Wu, V. Fong, A. Hsu, S. Chak, R. P. Naikawadi, P. J. Wolters, A. R. Abate, A. J. Butte, M. Bhattacharya, Reference-based analysis of lung single-cell sequencing reveals a transitional profibrotic macrophage. *Nat. Immunol.* **20**, 163–172 (2019).

44. Y. Lu, K. Li, Y. Hu, X. Wang, Expression of immune related genes and possible regulatory mechanisms in alzheimer's disease. *Front. Immunol.* **12**, 768966 (2021).

45. L. Li, H. Chen, D. Marin, Y. Xi, Q. Miao, J. Lv, P. P. Banerjee, H. Shaim, M. Daher, R. Basar, N. Imahashi, J. Jimenez, B. Hu, R. S. Mehta, L. N. Kerbauy, M. Kaplan, M. Mendt, G. Ozcan, E. Gokdemir, M. Hernandez Sanabria, Y. Li, K. Chen, J. Wang, L. Muniz-Feliciano, W.L. Zhao, R. E.

Champlin, E. J. Shpall, K. Rezvani, A novel immature natural killer cell subpopulation predicts relapse after cord blood transplantation. *Blood Adv.* **3**, 4117–4130 (2019).

46. H. Chen, M. C. Lau, M. T. Wong, E. W. Newell, M. Poidinger, J. Chen, Cytofkit: A bioconductor package for an integrated mass cytometry data analysis pipeline. *PLOS Comput. Biol.* **12**, e1005112 (2016).